Atmospheric Environment 92 (2014) 162–170

Contents lists available at ScienceDirect

Atmospheric Environment

journal homepage: www.elsevier.com/locate/atmosenv

Variation of secondary coatings associated with elemental carbon by single particle analysis

Guohua Zhang [a], Xinhui Bi [a,*], Junjie He [b], Duohong Chen [c], Lo Yin Chan [a], Guangwu Xie [c], Xinming Wang [a], Guoying Sheng [a], Jiamo Fu [a], Zhen Zhou [b]

[a] State Key Laboratory of Organic Geochemistry, Guangzhou Institute of Geochemistry, Chinese Academy of Sciences, Guangzhou 510640, PR China
[b] Department of Environmental Engineering, Jinan University, Guangzhou 510632, PR China
[c] State Environmental Protection Key Laboratory of Regional Air Quality Monitoring, Guangdong Environmental Monitoring Center, Guangzhou 510308, PR China

HIGHLIGHTS

- Secondary compositions associated with EC were observed with SPAMS in real time.
- EC-containing particles accounted for ~33% (21–50%), of total analyzed particles.
- EC was internally mixed with sulfate (97.4%), nitrate (89.5%), and ammonium (80%).
- Distinct diurnal cycle of the EC mixing state in condensation mode was observed.
- Photochemical aging may contribute to growth of smaller EC-containing particles.

ARTICLE INFO

Article history:
Received 8 December 2013
Received in revised form
3 April 2014
Accepted 10 April 2014
Available online 13 April 2014

Keywords:
Mixing state
Elemental carbon
Sulfate
Organics
Single particle
PRD

ABSTRACT

The mixing state of elemental carbon (EC) with secondary species has been highlighted as a major uncertainty in assessing its climate impact. However, the extent to which secondary coatings are present on EC and the underlying processes remained poorly understood in China, where there is a high loading of EC produced from extensive usage of fossil fuels and biomass. A single particle aerosol mass spectrometer (SPAMS) was applied to detect the chemical compositions associated with EC at the Guangdong Atmospheric Supersite, China. Efforts were made to track the variation of secondary coatings on EC. It is the first report on the direct observation of secondary compositions associated with EC with high time resolution in China. The hourly average number of EC-containing particles accounted for ~33% (21–50%) of total analyzed particles over the sampling period. EC was found to be extensively internally mixed with sulfate (97.4% in number), nitrate (89.5%), oxidized organics (69.6%), and/or ammonium (80%). The results also indicate that secondary processing on EC in condensation (0.2–0.5 μm) and droplet (0.7–1.1 μm) modes is different. Active photochemical formation of oxidized organics and ammonium sulfate during daytime, and formation of ammonium nitrate during nighttime led to a distinct diurnal circle of mixing state of EC in the condensation mode. However, the photochemical aging may have limited or negligible influence on the mixing state and growth of EC in the droplet mode. These findings improve the understanding of the evolution of physicochemical properties of EC, and may help to model its climate impact.

1. Introduction

Aerosols represent the largest uncertainty in estimating radiative forcing of atmospheric species, through strongly affecting the energy balance of the Earth by scattering and/or absorbing solar radiation (Pöschl, 2005), and influencing cloud formation (Jacobson, 2006). Generated exclusively by incomplete combustion of fossil fuel and biomass, elemental carbon (EC) represents a substantially important fraction of atmospheric aerosols (Chan and Yao, 2008) and imposes a strong positive forcing to the global climate. Recent studies suggested that EC may have a warming potential second only to CO_2 (e.g., Ramanathan and Carmichael, 2008).

* Corresponding author.
E-mail address: bixh@gig.ac.cn (X. Bi).

http://dx.doi.org/10.1016/j.atmosenv.2014.04.018
1352-2310/

Many studies have demonstrated that optical properties of EC are sensitive to their physical (e.g., size and morphology) and chemical (e.g., composition, mixing state) properties (Moffet and Prather, 2009). While freshly emitted EC may contain limited coating, atmospheric aging such as coagulation with other particles, condensation of vapors, and in-cloud processing could cause EC to internally mix with other chemical species (e.g., Moffet and Prather, 2009). Cappa et al. (2012) and Lan et al. (2013) had observed a limited enhancement due to the mixing state of ambient EC, however, other studies confirmed the enhancement effect of internally mixing under various conditions (Wei et al., 2013; Zhang et al., 2008). The internally mixing can result in enhanced absorption by nearly 2-fold and scattering capacity by approximately 10-fold at 80% relative humidity (RH) relative to fresh particles (Zhang et al., 2008).

The mixing state of individual EC particles is very complex and constantly changing in the atmosphere. Advances in on-line instrumentation have provided a direct measurement of size-resolved mixing state, and thus this could help to track the evolution of chemical compositions and their influence on the optical properties of aerosols with high time resolution. Volatility Tandem Differential Mobility Analyzer (VTDMA) and Single Particle Soot Photometer (SP2) can obtain the information on mixing state of refractory black carbon (rBC), in addition to mass quantification (Schwarz et al., 2006). Through the application of VTDMA, Cheng et al. (2009) observed significantly enhanced light scattering and absorption capacity of rBC due to the secondary processing of rBC in a polluted region of China. With a SP2, the rBC in the Pearl River Delta (PRD) region of China was also frequently found to be internally mixed with non-refractory materials (Huang et al., 2011, 2012). However, these measurements are based on the thermo or optical methods and thus they do not provide any chemical information. Single particle mass spectrometry (SPMS) can provides the details of chemical composition measurements for single particles, including EC (e.g., Cahill et al., 2012; Pratt and Prather, 2012 and references therein; Zauscher et al., 2013). For example, Moffet and Prather (2009) observed a rapid coating process of organic carbon (OC) and sulfate on the EC core and assessed the related absorption enhancement in the polluted atmosphere of the Mexico city. Healy et al. (2012) found that the mixing state of EC-containing particles showed dependency on vacuum aerodynamic diameter (d_{va}), with smaller particles ($d_{va} \leq 0.4$ μm) mainly externally mixed and larger particles ($d_{va} > 0.4$ μm) mainly internally mixed, influenced by sources and transport. Cahill et al. (2012) showed that majority of soot is internally mixed and temporally varied. The term EC is used herein, instead of BC or soot since the SPMS uses mass spectrometry as method of detection, rather than light absorption. The definitions of EC and BC have been discussed in details elsewhere (Bond and Bergstrom, 2006).

Previous studies demonstrated an important role of EC in atmospheric light extinction in the PRD region (e.g., Yu et al., 2010). However, the aerosol measurements of EC in China reported so far have been primarily based on bulk techniques (Wu et al., 2012) that could not provide sufficient information on compositions of EC-containing particles, including the coating materials at single particle level. The details of coating materials and their influence on the physicochemical properties of EC are still very limited in China. Additionally, the mechanisms governing transformation of EC from being externally to internally mixed are also unclear. In this study, both d_{va} and chemical compositions of ambient aerosols with high-time resolution in the PRD region, China were analyzed by a Single Particle Aerosol Mass Spectrometer (SPAMS) in order to improve the understanding on atmospheric aging processes of EC. EC-containing particles analyzed by SPAMS were in the size range of 0.2–1.2 μm, which is consistent with the dominant fraction of EC mass in the atmosphere of the PRD region (Huang et al., 2011, 2012). Variations of the most abundant secondary species (i.e., sulfate, organics, ammonium, and nitrate) associated with EC as a function of d_{va}, and also their diurnal trends are discussed.

2. Methods

2.1. Sampling site and ambient observation

Ambient measurements were conducted at Guangdong Atmospheric Supersite (22.73N, 112.93E), a suburban site of Heshan city in the PRD region, surrounded mainly by farm land (Fig. S1 in Supplementary material (SM)). The site is located on a hill with an elevation of 60 m, approximately 80 and 50 km downwind site to Guangzhou and Foshan, respectively, and both cities are densely industrial areas. A sampling inlet was set up on a building at approximately 15 m above the ground level. Continuous SPAMS measurements lasted approximately for 10 days, from 21st November to 1st December 2010. The details of single particle detection method can be found in the SM.

2.2. Data analysis procedure

A total of approximately 1,500,000 particles, with d_{va} in the size range of 0.2–1.2 μm, were chemically analyzed with both positive and negative ion spectra. Particles sizes and mass spectra were imported into MATLAB (The Mathworks Inc.) and further analyzed with YAADA (www.yaada.org), a MATLAB-based software toolkit for processing single-particle mass spectra. Single particles clustering was performed with adaptive resonance theory based neural network algorithm (ART-2a) (Song et al., 1999), based on the presence and intensities of ion peaks in individual mass spectra. Parameters applied in the algorithm were set as 0.7 (vigilance factor), 0.05 (learning rate), and 20 (iterations). The first 400 hundred of all clusters (2182) generated by ART-2a, accounting for ~95% of all analyzed particles, were further manually combined into 11 single particle types.

3. Results and discussion

3.1. Meteorological conditions and pollution level

Fig. 1 shows real-time (in 1 h resolution) meteorological data, including ambient temperature (Temp), RH and wind speed (WS), and concentrations of gaseous pollutants (SO_2, NO_x, and O_3), BC and $PM_{2.5}$. Ambient Temp and RH during the field study generally varied between 12 and 26 °C and 45–95%, with an average of 19 °C and 69%, respectively. BC, CO, and $PM_{2.5}$ similarly exhibited pronounced diurnal variation, with two major peaks during morning (8:00–10:00, local time) and night hours (19:00–23:00). The concentrations of BC and $PM_{2.5}$ varied in the ranges of 2.9–13.8 and 23.5–145.2 μg m^{-3}, with mean values of 8.2 and 74.6 μg m^{-3}, respectively. Their diurnal trend was likely associated with variations of traffic emission, wind speed and boundary layer. Relatively strong wind and higher boundary layer diffused the pollutions and eventually led to lower pollution levels during the daytime, however, light wind enhanced pollution in a thinner boundary layer after sunset (Fan et al., 2008, 2011). The meteorological conditions during the nighttime facilitated the accumulation of pollutants, with frequently observed high level of $PM_{2.5}$ (>75 μg m^{-3}). According to back-trajectory analysis (more details can be found in the SM), air masses from northeastern continental areas dominated over the sampling period. Many short and circled back trajectories

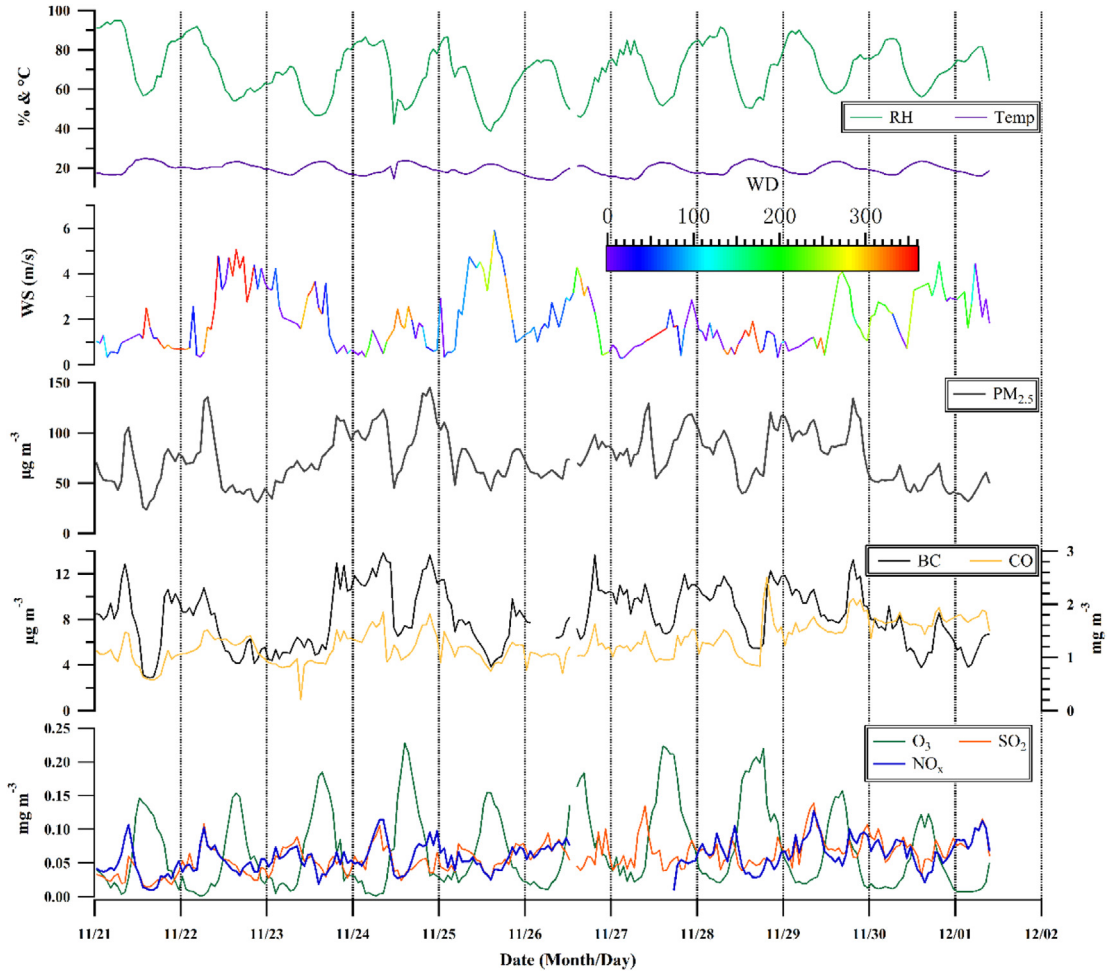

Fig. 1. Temporal profiles (in 1 h resolution) of $PM_{2.5}$ and BC mass concentrations, gaseous pollutants (SO_2, NO_x, and O_3, CO) and selected meteorological parameters (temperature (Temp)), relative humidity (RH), wind direction (WD), and wind speed (WS), provided by Guangdong Environmental Monitoring Center (http://www.gdemc.gov.cn/) during 11/21–12/02, 2010. The concentrations of $PM_{2.5}$ and BC were continuously measured using a tapered element oscillating microbalance (TEOM 1405, Thermo Scientific) and a Multiangle Absorption Photometer (Model 5012, Thermo Scientific) co-located at the site, respectively.

were observed (Fig. S2), which implies that air pollution was strongly influenced by regional processes.

3.2. General characteristics of EC-containing particles

The particle types with their number fractions throughout the sampling period are listed in Table S1, and their average mass spectra are shown in Fig. S3. EC-containing particles are defined as combination of ECOC and EC particle types that contained intense ion signals from EC. Representative ion peaks for EC-containing particles, as presented in Fig. 2, are EC cluster ions (e.g., m/z ±12 $[C]^{+/-}$, ±36$[C_3]^{+/-}$, ±48$[C_4]^{+/-}$ and ±60$[C_5]^{+/-}$), OC fragments (m/z 27$[C_2H_3]^+$, 29$[C_2H_5]^+$, 37$[C_3H]^+$, and 43$[C_2H_3O]^+$), and secondary inorganic species (SIS), such as sulfate (−97$[HSO_4]^-$, −80$[SO_3]^-$), nitrate (−62$[HNO_3]^-$, −46$[NO_2]^-$), and ammonium (18$[NH_4]^+$). An occurrence of intense 39$[K]^+$ ion peak associated with ion peaks due to −26$[CN]^-$ and −42$[CNO]^-$ indicates the contribution of biomass/biofuel burning (e.g., Bi et al., 2011; Pratt et al., 2011; Silva et al., 1999). There are also some other metallic species such as 23 $[Na]^+$, 51$[V]^+$/67$[VO]^+$, 56$[Fe]^+$ and 206–208$[Pb]^+$.

The hourly average number of EC-containing particles accounted for ~33% (21–50%) of the total analyzed particles. The EC-containing particles were also observed at a high number fraction (>30%) in other regions over the world (Cahill et al., 2012; Fu et al., 2012; Hasegawa and Ohta, 2002). It is noted that this is a conservative estimation since minor fraction of EC may still associate with other particle types (e.g., Biomass particles in Fig. S3). It is due to interference of other species which are highly sensitive to the laser beam and thus generated suppressive ion peaks, such as potassium in Biomass particles (Gross et al., 2000). On average, the number fraction of EC-containing particles (Nf_{EC}, relative to total analyzed particles in the same size range throughout the study) was highly variable with d_{va} (Table 1). It represented the dominant fraction (~70%) in the size range of 0.2–0.3 μm, and decreased to ~30% for larger particles (>0.5 μm). The distribution pattern is generally consistent with our previous study conducted in an urban area of the PRD region (Zhang et al., 2013a).

According to a correlation analysis of the temporal variation (in 1-h resolution) of number count in 0.1 μm width, as listed in Table 1, condensation (d_{va} = 0.2–0.5 μm) (Group 1) and droplet modes (d_{va} = 0.7–1.1 μm) (Group 3) of EC were extracted, which represented the typical modes distribution of EC mass in the PRD region (Huang and Yu, 2008). The number count of EC-containing particles in each mode correlated with each other ($r > 0.6$, $p < 0.001$), but the correlation between the groups was weak. The remaining group (Group 2) located in d_{va} = 0.5–0.7 μm was supposed to be an intersection of these two modes, and therefore was not included in the discussion. Presence of the condensation mode is consistent

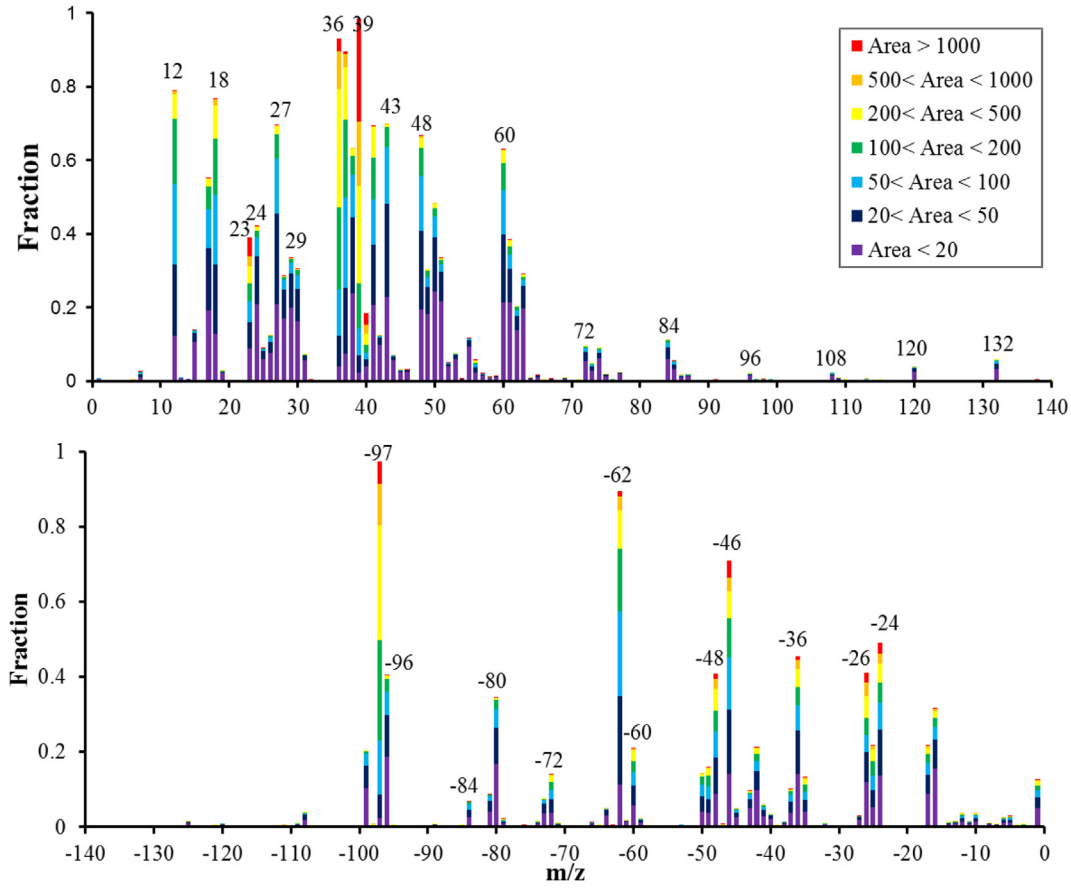

Fig. 2. A digital color stack for the positive (upper) and negative (bottom) mass spectra of EC-containing particles, showing the fraction of particles containing a specific peak on the *y*-axis versus mass-to-charge on the *x*-axis. The color represents the fraction in a specific range of peak areas.

Table 1
Size-resolved number count, and fraction of EC-containing particles, relative to total analyzed particles of the same size range, and correlation analysis of the temporal variation of EC in each size bin (in 100 nm resolution) throughout the entire field study.

	BC	EC[a]	Group 1 EC[c]			Group 2 EC			Group 3 EC			
			[0.2–0.3][b]	**[0.3–0.4]**	**[0.4–0.5]**	*[0.5–0.6]*	*[0.6–0.7]*	***[0.7–0.8]***	***[0.8–0.9]***	***[0.9–1.0]***	***[1.0–1.1]***	***[1.1–1.2]***
BC												
EC	−0.08											
[0.2–0.3]	***0.54***	0.08										
[0.3–0.4]	***0.60***	0.06	0.79									
[0.4–0.5]	***0.60***	0.24	0.59	0.65								
[0.5–0.6]	−0.10	***0.91***	−0.07	−0.11	0.15							
[0.6–0.7]	−0.43	***0.66***	−0.17	−0.24	−0.33	0.51						
[0.7–0.8]	−0.34	0.29	−0.17	−0.21	−0.41	0.07	0.79					
[0.8–0.9]	−0.27	0.15	−0.15	−0.18	−0.41	−0.05	0.69	***0.92***				
[0.9–1.0]	−0.19	0.11	−0.10	−0.14	−0.35	−0.09	0.59	***0.85***	***0.87***			
[1.0–1.1]	−0.09	0.03	−0.09	−0.09	−0.31	−0.17	0.50	***0.80***	***0.80***	***0.79***		
[1.1–1.2]	0.01	0.00	−0.02	−0.03	−0.26	−0.18	0.40	***0.67***	***0.67***	***0.66***	***0.78***	
Count (#)		553,826	4471	10,700	139,238	260,855	92,532	29,602	10,028	3976	1672	752
Nf_{EC}			0.67	0.48	0.33	0.32	0.31	0.32	0.31	0.31	0.29	0.26

[a] The number of all the EC-containing particles.
[b] The number of EC-containing particles in each size bin.
[c] The groups of EC-containing particles were assigned according to the results from correlation analysis. The font types indicate different groups for EC-containing particles in different size ranges.

with the size distribution of EC in a roadway tunnel in this region, representing a relatively fresh emission (Huang and Yu, 2008; Huang et al., 2006). Through theoretical analysis, Huang and Yu (2008) suggested that in-cloud processing is a main reason for the presence of EC in the droplet mode, rather than coagulation, vapor condensation and/or hygroscopic growth in the PRD region. Study in this region also revealed that urban EC had a dominant condensation mode and a less abundant droplet mode, while the suburban/rural EC had a prominent mode in the droplet mode, due to the growth of smaller particles when the air mass moved from the urban source regions to the suburban/rural site (Yu et al., 2010). In Paris, Healy et al. (2012) showed that EC in the droplet mode,

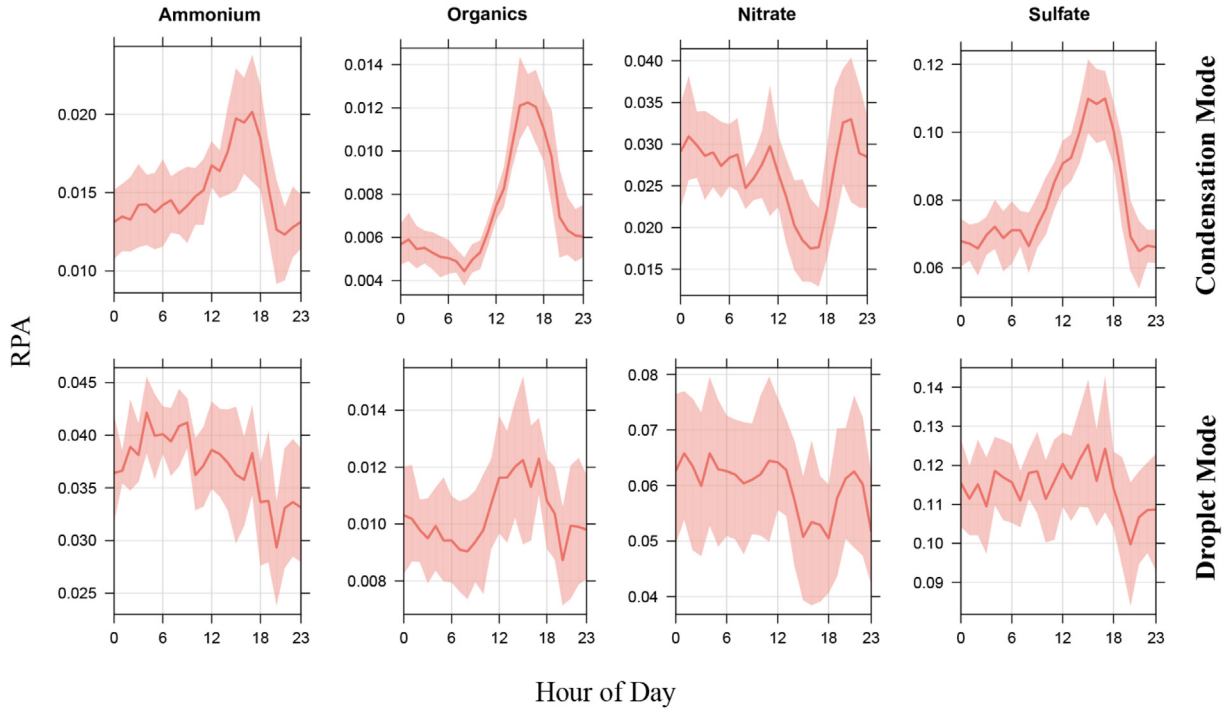

Fig. 3. Diurnal variation of RPAs of secondary species associated with EC-containing particles in the condensation (upper) and droplet modes (bottom). The light pink cover indicates the standard deviation. (For interpretation of the references to colour in this figure legend, the reader is referred to the web version of this article.)

dominated by aged, internally mixed particles, associated with continental transport events. However, temporal variation of EC-containing particles in the condensation mode closely tracked that of BC ($r = 0.64$, $p < 0.001$), indicating that condensation mode EC represents a major fraction of BC at the site.

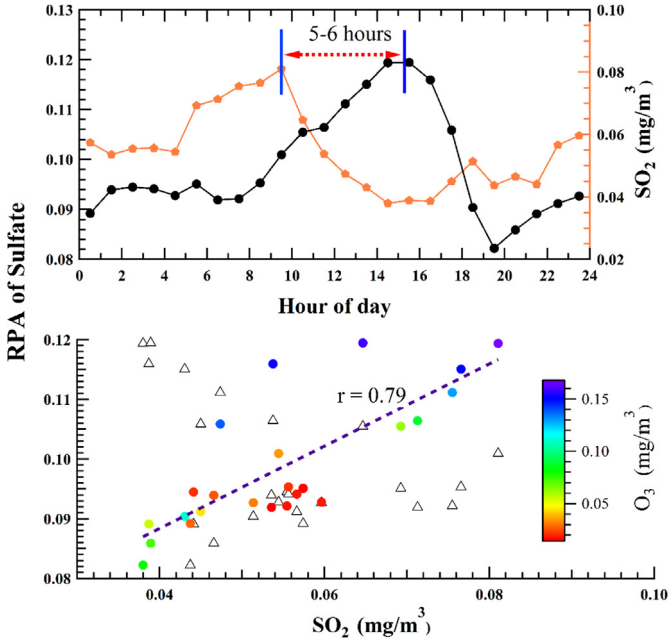

Fig. 4. Diurnal variation of SO_2 and RPA of sulfate on EC-containing particles (upper), and correlation between them (bottom). The triangles were plotted as RPA of sulfate versus SO_2, while the circles as RPA of sulfate versus SO_2 with 5 h delay, and the coloration indicates the concentration of O_3.

3.3. Diurnal variation of secondary coatings

Despite of matrix effects on the laser desorption/ionization for SPAMS, advances have been made in quantifying individual chemical species, either through multivariate analysis or by applying peak intensities for specific ions (e.g., Healy et al., 2013; Jeong et al., 2011; Xing et al., 2011). Relative peak area (RPA), defined as the peak area of each m/z divided by the total dual ion mass spectral peak area, is related to the relative amount of a species on a particle. Compared to absolute peak area, RPA was commonly applied because it is less sensitive to the variability in ion intensities associated with particle–laser interactions (Gross et al., 2000). The EC particles were found to be extensively internally mixed with detectable sulfate (97.4%), nitrate (89.5%), oxidized organics (69.6%), and/or ammonium (80%) (Fig. 2), indicative of the aging state for EC. Observation in California revealed that majority of EC-containing particles are internally mixed and are heavily influenced by secondary species (Cahill et al., 2012), primarily with secondary (oxidized) organic carbon and sulfate in the summer; whereas in the fall, they were mixed mostly with ammonium nitrate (Qin et al., 2012). The different mixing state of EC in this study can be attributed to various reasons (e.g., source and atmospheric processes). These results reveal that hydrophobic EC was commonly coated and/or coagulated with hygroscopic secondary materials in the atmosphere of the PRD region, which is consistent with previous studies in the same region (Zhang et al., 2013a), Yangtze River Delta region (Huang et al., 2013), northern China (Li et al., 2011) and Mexico city (Adachi and Buseck, 2008; Moffet and Prather, 2009). These hygroscopic coatings on EC particles can amplify their light absorption and growth through the absorption of water, and thus may lead to a greater effect on the formation of haze and regional climate. The study was focused on the variation of mixing state of EC with SIS and oxidized organics by RPA method. In SPMS studies, the m/z 43$[C_2H_3O]^+$ is commonly attributed to the oxidized

organics that are formed through photochemical processing (Qin et al., 2012). Secondary species, such as sulfate, oxidized organics, nitrate and ammonium represent the most abundant components of fine particles (Tao et al., 2012; Zhang et al., 2013b), and their formation is active during the fall in the PRD region (He et al., 2011).

The diurnal variations of RPAs of the secondary species associated with EC in the condensation and droplet modes are compared in Fig. 3. For the condensation mode, RPAs of sulfate, ammonium and oxidized organics exhibited pronounced diurnal variation, increasing gradually after sunrise, peaking in the afternoon, and decreasing gradually thereafter to a relatively stable level during nighttime. Totally different from these species, the RPA of nitrate associated with EC in the condensation mode usually showed a night or morning peak.

The diurnal variation trends of sulfate, ammonium and oxidized organics were highly correlated with that of O_3 during daytime (Fig. S4). It implies that photochemical aging leads to the increased fraction of ammonium, sulfate, and oxidized organics on EC. Photochemical processing of fresh fractal EC emitted in the early morning to form highly aged one, internally mixed with OC, ammonium, sulfate and nitrate in the afternoon has been directly observed in Mexico City (Moffet and Prather, 2009). The active photochemical formation of sulfate and oxidized organics during the daytime (Seinfeld and Pandis, 2006; Xiao et al., 2009) and high correlation between oxidized organics, sulfate, and O_3 have been observed with Aerosol Mass Spectrometer in the PRD and other regions (He et al., 2011; Jimenez et al., 2009). Huang et al. (2011) have observed a lower fraction of internally mixed EC during the nighttime than the daytime, and attributed it to the stronger

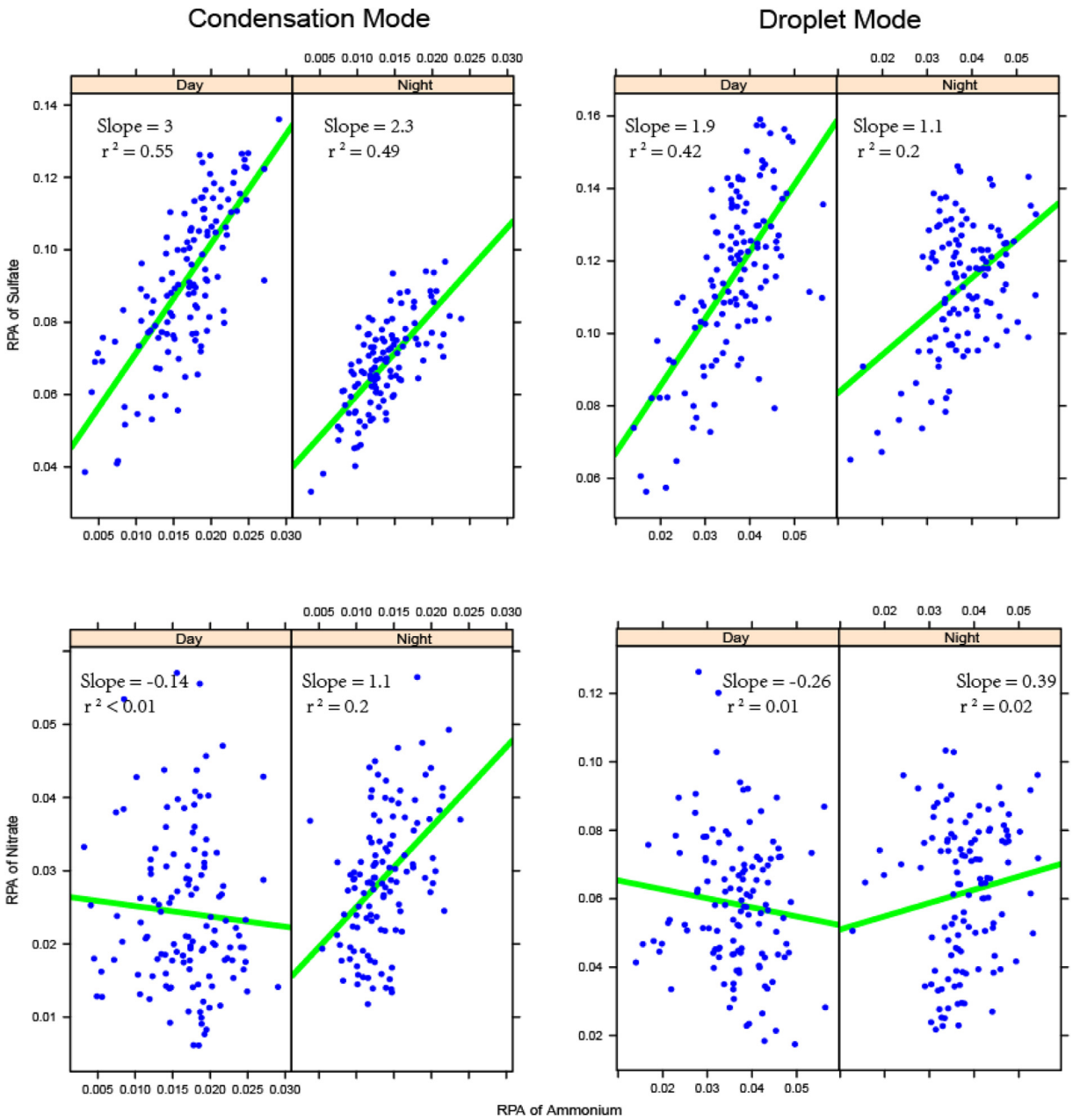

Fig. 5. Correlation analysis of RPAs of sulfate and nitrate with that of ammonium, associated with EC, in both the condensation (left column) and droplet modes (right column), respectively.

emission of fresh externally mixed EC during rush hours. The results in this study further indicate that formation of high abundant sulfate, ammonium and oxidized organics contributed to the extensively internally mixed EC during the afternoon. The analysis also suggests that EC can serve as an effective sink for sulfuric acid and oxidized organics in the atmosphere of the PRD region. Laboratory experiments and model simulation have revealed that condensation of sulfuric acid represents the dominant aging process of EC in the ambient atmosphere that proceeded on a time scale of several hours (Khalizov et al., 2009; Riemer et al., 2004). Evidence for the temporal profile of SO_2, which typically showed a morning peak and decreased with increasing O_3, and the diurnal variation of SO_2 and RPA of sulfate (Fig. 4) support the major pathway of sulfate from the photochemical oxidation of SO_2. The profile of O_3 applied herein to represent that of OH radical, whose concentration was unavailable (more details were provided in the SM). The correlation between the concentration of SO_2 and the RPA of sulfate is considerably improved when the average diurnal trend of SO_2 was shifted to 5 h later. This time gap might be required to effectively produce sulfate from the oxidation of SO_2. The associated sulfate on EC cores should be in a form of ammonium sulfate, indicated from the correlation analysis shown in Fig. 5. The trend for nitrate could be explained by the heterogeneous uptake of N_2O_5 or condensation of ammonium nitrate onto the EC cores (Hu et al., 2008; Lee et al., 2003; Wang et al., 2009). The correlation between RPAs of ammonium and nitrate (Fig. 5) supported the condensation of ammonium nitrate. Occasionally, nitrate also peaked in late morning, similar to the observation by Lee et al. (2003), which is attributed to gas-phase oxidation of NO_2 with OH radicals, followed by condensation of HNO_3 (Seinfeld and Pandis, 2006).

For the droplet mode, the diurnal trends of RPAs of sulfate, ammonium, oxidized organics and nitrate associated with EC exhibits little dependence upon time of day, indicating some other mechanisms (e.g., in-cloud processing as discussed above). Fig. 5 also showed that sulfate was in a form of ammonium sulfate in the droplet mode. However, there was no relevance between ammonium and nitrate, which may suggest that heterogeneous reactions are involved in the formation of nitrate in the droplet mode.

3.4. Size dependence of secondary coatings

The distribution of RPAs of SIS and oxidized organics (43 $[C_2H_3O]^+$) along d_{va} is displayed in Fig. 6. Although EC was commonly internally mixed with SIS and oxidized organics, the pattern implies that the distribution of these secondary species was actually highly dependent on d_{va}. The average RPAs of the secondary species commonly increased towards larger particles, suggesting that the formation of secondary species directly contributed to the growth of EC particles. These were consistent with previous atmospheric observations conducted in Vienna, Austria (Okada and Hitzenberger, 2001), and Sapporo, Japan (Hasegawa and Ohta, 2002). Fig. 6 shows that the RPA of nitrate on EC increased with d_{va}, however, the RPAs of ammonium, sulfate and 43$[C_2H_3O]^+$ only increased in the condensation mode, and remained relatively stable in the droplet mode. It can be explained by their different formation mechanisms, as mentioned above (section 3.3). The size dependence of sulfate and ammonium is strongly related, which is consistent with the results presented in Fig. 5 that sulfate predominantly associated with ammonium. The distribution of nitrate showed less dependence on ammonium in the droplet mode, also consistent with the correlation analysis in Fig. 5. The results further support that nitrate on EC was mainly formed from the condensation of nitric acid rather than ammonium nitrate on EC in the droplet mode (Wang et al., 2009).

Evidence further showed that the addition of secondary species directly contributed to the growth of EC-containing particles during the noon. The difference between size distributions of EC-

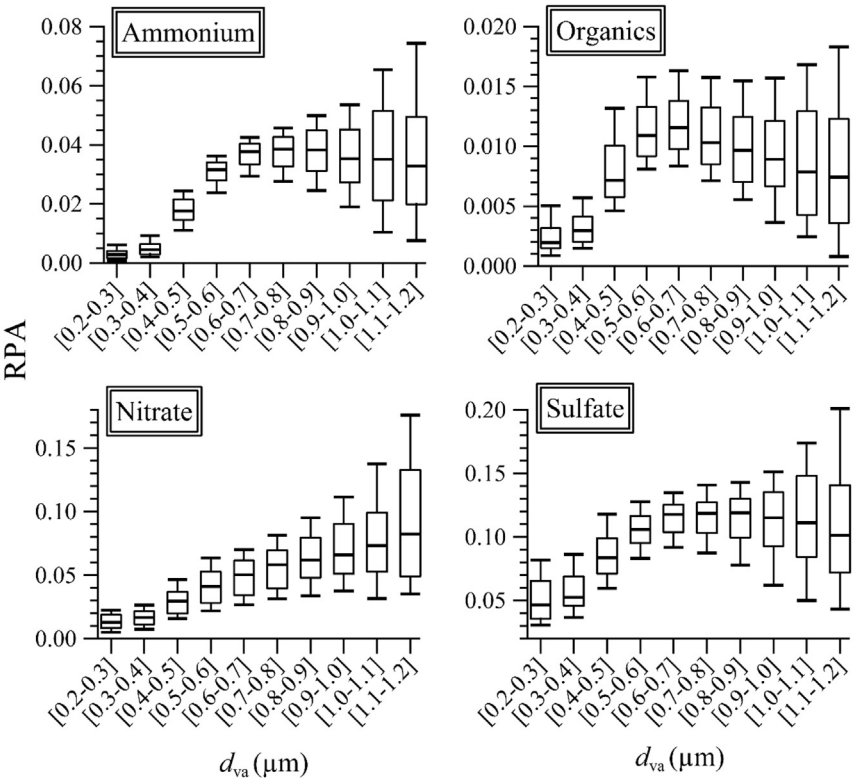

Fig. 6. Variation of RPAs of secondary species on EC-containing particles as a function of d_{va}.

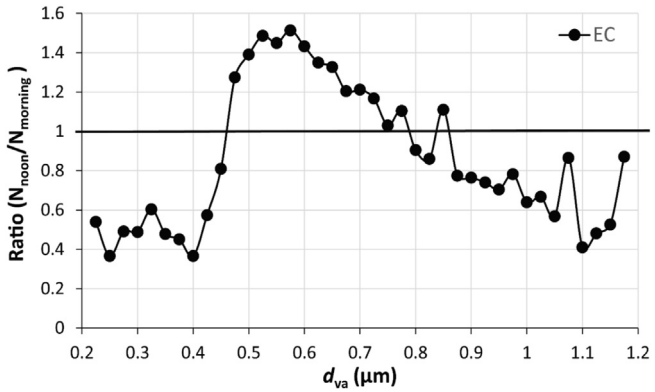

Fig. 7. Variation of number count Ratio (noon hours/morning hours) for EC-containing particles with d_{va}.

containing particles during morning and afternoon hours in Fig. S5 showed that the count of EC-containing particles in smaller particles (0.2–0.4 μm) was more abundant during nighttime and morning hours. It may suggest that EC-containing particles in the smaller particles were transformed into larger particles as the photochemical aging. The difference is more specifically displayed in Fig. 7, as size dependent ratios of EC during morning and afternoon hours. The ratios of number counts of EC-containing particles during noon (11:00–15:00) to morning hours (7:00–10:00) showed a decrease in the condensation mode. It was ~0.4–0.6 and ~1.5 in smaller (0.2–0.4 μm) and larger particles (0.5–0.6 μm), respectively, which implies that the particle growth dominated over primary emission during the noon period. In the droplet mode, the ratio slightly decreased with increasing d_{va}, which may be associated with higher boundary layer during the afternoon, and also the evaporation of semi-volatile species.

4. Conclusions

Direct observation of size-resolved mixing state of individual EC was performed during the fall of 2010 in the PRD region, China. EC-containing particles accounted for ~33% (21–50%), highly depending on the particle size. Ambient EC particles were commonly internally mixed with secondary species such as oxidized organics, ammonium sulfate, and nitrate. The results from the analysis of these species associated with EC highlight the dependence of secondary coatings on the photochemical conditions and d_{va}. Active photochemical formation of oxidized organics and ammonium sulfate during the daytime, and condensation of ammonium nitrate during the nighttime led to the distinct diurnal circle of mixing state of EC in the condensation mode. However, the photochemical aging may have limited or negligible influence on the mixing state and the growth of EC in the droplet mode. The degree of internal mixing for EC showed an increase trend with d_{va} due to the coating of secondary species. While our observation may be insufficient to explain the amount of secondary species on EC as a function of d_{va}, the results still have an advantage to provide qualitative and comprehensive information on the size and time dependent trends of secondary coating on EC. These facts provide a reference for estimating their contribution to both light extinction in the PRD region, and also should be taken into account for reducing the uncertainty in regional aerosol-climate modeling of EC.

Acknowledgment

This work was supported by "Strategic Priority Research Program (B)" of the Chinese Academy of Sciences (XDB05020205), State Key Laboratory of Organic Geochemistry (SKLOG2013A01), and Youth Innovation Promotion Association, CAS. The authors also gratefully acknowledge the NOAA Air Resources Laboratory (ARL) for the provision of the HYSPLIT transport and dispersion model and/or READY website (http://ready.arl.noaa.gov) used in this publication. This is contribution from CASGIG 1850.

Appendix A. Supplementary data

Supplementary data related to this article can be found at http://dx.doi.org/10.1016/j.atmosenv.2014.04.018.

References

Adachi, K., Buseck, P.R., 2008. Internally mixed soot, sulfates, and organic matter in aerosol particles from Mexico City. Atmospheric Chemistry And Physics 8, 6469–6481.

Bi, X.H., Zhang, G.H., Li, L., Wang, X.M., Li, M., Sheng, G.Y., Fu, J.M., Zhou, Z., 2011. Mixing state of biomass burning particles by single particle aerosol mass spectrometer in the urban area of PRD, China. Atmospheric Environment 45, 3447–3453. http://dx.doi.org/10.1016/j.atmosenv.2011.03.034.

Bond, T.C., Bergstrom, R.W., 2006. Light absorption by carbonaceous particles: an investigative review. Aerosol Science and Technology 40, 27–67. http://dx.doi.org/10.1080/02786820500421521.

Cahill, J.F., Suski, K., Seinfeld, J.H., Zaveri, R.A., Prather, K.A., 2012. The mixing state of carbonaceous aerosol particles in northern and southern California measured during CARES and CalNex 2010. Atmospheric Chemistry And Physics 12, 10989–11002. http://dx.doi.org/10.5194/acp-12-10989-2012.

Cappa, C.D., Onasch, T.B., Massoli, P., Worsnop, D.R., Bates, T.S., Cross, E.S., Davidovits, P., Hakala, J., Hayden, K.L., Jobson, B.T., Kolesar, K.R., Lack, D.A., Lerner, B.M., Li, S.M., Mellon, D., Nuaaman, I., Olfert, J.S., Petaja, T., Quinn, P.K., Song, C., Subramanian, R., Williams, E.J., Zaveri, R.A., 2012. Radiative absorption enhancements due to the mixing state of atmospheric black carbon. Science 337, 1078–1081. http://dx.doi.org/10.1126/science.1223447.

Chan, C.K., Yao, X., 2008. Air pollution in mega cities in China. Atmospheric Environment 42, 1–42. http://dx.doi.org/10.1016/j.atmosenv.2007.09.003.

Cheng, Y.F., Berghof, M., Garland, R.M., Wiedensohler, A., Wehner, B., Muller, T., Su, H., Zhang, Y.H., Achtert, P., Nowak, A., Poschl, U., Zhu, T., Hu, M., Zeng, L.M., 2009. Influence of soot mixing state on aerosol light absorption and single scattering albedo during air mass aging at a polluted regional site in northeastern China. Journal of Geophysical Research-Atmospheres 114, D00G10. http://dx.doi.org/10.1029/2008jd010883.

Fan, S., Wang, B., Tesche, M., Engelmann, R., Althausen, A., Liu, J., Zhu, W., Fan, Q., Li, M., Ta, N., Song, L., Leong, K., 2008. Meteorological conditions and structures of atmospheric boundary layer in October 2004 over Pearl River Delta area. Atmospheric Environment 42, 6174–6186.

Fan, S.J., Fan, Q., Yu, W., Luo, X.Y., Wang, B.M., Song, L.L., Leong, K.L., 2011. Atmospheric boundary layer characteristics over the Pearl River Delta, China, during the summer of 2006: measurement and model results. Atmospheric Chemistry And Physics 11, 6297–6310. http://dx.doi.org/10.5194/acp-11-6297-2011.

Fu, H., Zhang, M., Li, W., Chen, J., Wang, L., Quan, X., Wang, W., 2012. Morphology, composition and mixing state of individual carbonaceous aerosol in urban Shanghai. Atmospheric Chemistry And Physics 12, 693–707. http://dx.doi.org/10.5194/acp-12-693-2012.

Gross, D.S., Galli, M.E., Silva, P.J., Prather, K.A., 2000. Relative sensitivity factors for alkali metal and ammonium cations in single particle aerosol time-of-flight mass spectra. Analytical Chemistry 72, 416–422.

Hasegawa, S., Ohta, S., 2002. Some measurements of the mixing state of soot-containing particles at urban and non-urban sites. Atmospheric Environment 36, 3899–3908.

He, L.Y., Huang, X.F., Xue, L., Hu, M., Lin, Y., Zheng, J., Zhang, R.Y., Zhang, Y.H., 2011. Submicron aerosol analysis and organic source apportionment in an urban atmosphere in Pearl River Delta of China using high-resolution aerosol mass spectrometry. Journal of Geophysical Research-Atmospheres 116, D12304. http://dx.doi.org/10.1029/2010jd014566.

Healy, R.M., Sciare, J., Poulain, L., Crippa, M., Wiedensohler, A., Prevot, A.S.H., Baltensperger, U., Sarda-Esteve, R., McGuire, M.L., Jeong, C.H., McGillicuddy, E., O'Connor, I.P., Sodeau, J.R., Evans, G.J., Wenger, J.C., 2013. Quantitative determination of carbonaceous particle mixing state in Paris using single-particle mass spectrometer and aerosol mass spectrometer measurements. Atmospheric Chemistry And Physics 13, 9479–9496. http://dx.doi.org/10.5194/acp-13-9479-2013.

Healy, R.M., Sciare, J., Poulain, L., Kamili, K., Merkel, M., Muller, T., Wiedensohler, A., Eckhardt, S., Stohl, A., Sarda-Esteve, R., McGillicuddy, E., O'Connor, I.P., Sodeau, J.R., Wenger, J.C., 2012. Sources and mixing state of size-resolved elemental carbon particles in a European megacity: Paris. Atmospheric Chemistry And Physics 12, 1681–1700. http://dx.doi.org/10.5194/acp-12-1681-2012.

Hu, M., Wu, Z., Slanina, J., Lin, P., Liu, S., Zeng, L., 2008. Acidic gases, ammonia and water-soluble ions in PM2.5 at a coastal site in the Pearl River Delta, China. Atmospheric Environment 42, 6310–6320.

Huang, X.F., Gao, R.S., Schwarz, J.P., He, L.Y., Fahey, D.W., Watts, L.A., McComiskey, A., Cooper, O.R., Sun, T.L., Zeng, L.W., Hu, M., Zhang, Y.H., 2011. Black carbon measurements in the Pearl River Delta region of China. Journal of Geophysical Research 116, D12208. http://dx.doi.org/10.1029/2010jd014933.

Huang, X.F., Sun, T.L., Zeng, L.W., Yu, G.H., Luan, S.J., 2012. Black carbon aerosol characterization in a coastal city in South China using a single particle soot photometer. Atmospheric Environment 51, 21–28. http://dx.doi.org/10.1016/j.atmosenv.2012.01.056.

Huang, X.F., Xue, L., Tian, X.D., Shao, W.W., Sun, T.L., Gong, Z.H., Ju, W.W., Jiang, B., Hu, M., He, L.Y., 2013. Highly time-resolved carbonaceous aerosol characterization in Yangtze River Delta of China: composition, mixing state and secondary formation. Atmospheric Environment 64, 200–207. http://dx.doi.org/10.1016/j.atmosenv.2012.09.059.

Huang, X.F., Yu, J.Z., 2008. Size distributions of elemental carbon in the atmosphere of a coastal urban area in South China: characteristics, evolution processes, and implications for the mixing state. Atmospheric Chemistry And Physics 8, 5843–5853.

Huang, X.F., Yu, J.Z., He, L.Y., Hu, M., 2006. Size distribution characteristics of elemental carbon emitted from Chinese vehicles: results of a tunnel study and atmospheric implications. Environmental Science & Technology 40, 5355–5360.

Jacobson, M.Z., 2006. Effects of externally-through-internally-mixed soot inclusions within clouds and precipitation on global climate. Journal of Physical Chemistry A 110, 6860–6873. http://dx.doi.org/10.1021/Jp056391r.

Jeong, C.H., McGuire, M.L., Godri, K.J., Slowik, J.G., Rehbein, P.J.G., Evans, G.J., 2011. Quantification of aerosol chemical composition using continuous single particle measurements. Atmospheric Chemistry And Physics 11, 7027–7044. http://dx.doi.org/10.5194/acp-11-7027-2011.

Jimenez, J.L., Canagaratna, M.R., Donahue, N.M., Prevot, A.S.H., Zhang, Q., Kroll, J.H., DeCarlo, P.F., Allan, J.D., Coe, H., Ng, N.L., Aiken, A.C., Docherty, K.S., Ulbrich, I.M., Grieshop, A.P., Robinson, A.L., Duplissy, J., Smith, J.D., Wilson, K.R., Lanz, V.A., Hueglin, C., Sun, Y.L., Tian, J., Laaksonen, A., Raatikainen, T., Rautiainen, J., Vaattovaara, P., Ehn, M., Kulmala, M., Tomlinson, J.M., Collins, D.R., Cubison, M.J., Dunlea, E.J., Huffman, J.A., Onasch, T.B., Alfarra, M.R., Williams, P.I., Bower, K., Kondo, Y., Schneider, J., Drewnick, F., Borrmann, S., Weimer, S., Demerjian, K., Salcedo, D., Cottrell, L., Griffin, R., Takami, A., Miyoshi, T., Hatakeyama, S., Shimono, A., Sun, J.Y., Zhang, Y.M., Dzepina, K., Kimmel, J.R., Sueper, D., Jayne, J.T., Herndon, S.C., Trimborn, A.M., Williams, L.R., Wood, E.C., Middlebrook, A.M., Kolb, C.E., Baltensperger, U., Worsnop, D.R., 2009. Evolution of organic aerosols in the atmosphere. Science 326, 1525–1529. http://dx.doi.org/10.1126/science.1180353.

Khalizov, A.F., Zhang, R.Y., Zhang, D., Xue, H.X., Pagels, J., McMurry, P.H., 2009. Formation of highly hygroscopic soot aerosols upon internal mixing with sulfuric acid vapor. Journal of Geophysical Research-Atmospheres 114, D05208. http://dx.doi.org/10.1029/2008jd010595.

Lan, Z.J., Huang, X.F., Yu, K.Y., Sun, T.L., Zeng, L.W., Hu, M., 2013. Light absorption of black carbon aerosol and its enhancement by mixing state in an urban atmosphere in South China. Atmospheric Environment 69, 118–123. http://dx.doi.org/10.1016/j.atmosenv.2012.12.009.

Lee, S.H., Murphy, D.M., Thomson, D.S., Middlebrook, A.M., 2003. Nitrate and oxidized organic ions in single particle mass spectra during the 1999 Atlanta Supersite Project. Journal of Geophysical Research 108, 8417. http://dx.doi.org/10.1029/2001jd001455.

Li, W., Zhou, S., Wang, X., Xu, Z., Yuan, C., Yu, Y., Zhang, Q., Wang, W., 2011. Integrated evaluation of aerosols from regional brown hazes over northern China in winter: concentrations, sources, transformation, and mixing states. Journal of Geophysical Research 116, D09301. http://dx.doi.org/10.1029/2010jd015099.

Moffet, R.C., Prather, K.A., 2009. In-situ measurements of the mixing state and optical properties of soot with implications for radiative forcing estimates. Proceedings of the National Academy of Sciences of the United States of America 106, 11872–11877. http://dx.doi.org/10.1073/pnas.0900040106.

Okada, K., Hitzenberger, R.M., 2001. Mixing properties of individual submicrometer aerosol particles in Vienna. Atmospheric Environment 35, 5617–5628.

Pöschl, U., 2005. Atmospheric aerosols: composition, transformation, climate and health effects. Angewandte Chemie International Edition 44, 7520–7540.

Pratt, K.A., Murphy, S.M., Subramanian, R., DeMott, P.J., Kok, G.L., Campos, T., Rogers, D.C., Prenni, A.J., Heymsfield, A.J., Seinfeld, J.H., Prather, K.A., 2011. Flight-based chemical characterization of biomass burning aerosols within two prescribed burn smoke plumes. Atmospheric Chemistry And Physics 11, 12549–12565. http://dx.doi.org/10.5194/acp-11-12549-2011.

Pratt, K.A., Prather, K.A., 2012. Mass spectrometry of atmospheric aerosols recent developments and applications. Part II: on-line mass spectrometry techniques. Mass Spectrometry Reviews 31, 17–48. http://dx.doi.org/10.1002/Mas.20330.

Qin, X.Y., Pratt, K.A., Shields, L.G., Toner, S.M., Prather, K.A., 2012. Seasonal comparisons of single-particle chemical mixing state in Riverside, CA. Atmospheric Environment 59, 587–596. http://dx.doi.org/10.1016/j.atmosenv.2012.05.032.

Ramanathan, V., Carmichael, G., 2008. Global and regional climate changes due to black carbon. Nature Geoscience 1, 221–227. http://dx.doi.org/10.1038/Ngeo156.

Riemer, N., Vogel, H., Vogel, B., 2004. Soot aging time scales in polluted regions during day and night. Atmospheric Chemistry And Physics 4, 1885–1893.

Schwarz, J.P., Gao, R.S., Fahey, D.W., Thomson, D.S., Watts, L.A., Wilson, J.C., Reeves, J.M., Darbeheshti, M., Baumgardner, D.G., Kok, G.L., Chung, S.H., Schulz, M., Hendricks, J., Lauer, A., Karcher, B., Slowik, J.G., Rosenlof, K.H., Thompson, T.L., Langford, A.O., Loewenstein, M., Aikin, K.C., 2006. Single-particle measurements of midlatitude black carbon and light-scattering aerosols from the boundary layer to the lower stratosphere. Journal of Geophysical Research-Atmospheres 111, D16207. http://dx.doi.org/10.1029/2006jd007076.

Seinfeld, J.H., Pandis, S.N., 2006. Atmospheric Chemistry and Physics: from Air Pollution to Climate Change, New Jersey.

Silva, P.J., Liu, D.Y., Noble, C.A., Prather, K.A., 1999. Size and chemical characterization of individual particles resulting from biomass burning of local Southern California species. Environmental Science & Technology 33, 3068–3076.

Song, X.H., Hopke, P.K., Fergenson, D.P., Prather, K.A., 1999. Classification of single particles analyzed by ATOFMS using an artificial neural network, ART-2A. Analytical Chemistry 71, 860–865.

Tao, J., Shen, Z.X., Zhu, C.S., Yue, J.H., Cao, J.J., Liu, S.X., Zhu, L.H., Zhang, R.J., 2012. Seasonal variations and chemical characteristics of sub-micrometer particles (PM1) in Guangzhou, China. Atmospheric Research 118, 222–231. http://dx.doi.org/10.1016/j.atmosres.2012.06.025.

Wang, X.F., Zhang, Y.P., Chen, H., Yang, X., Chen, J.M., Geng, F.H., 2009. Particulate nitrate formation in a highly polluted urban area: a case study by single-particle mass spectrometry in Shanghai. Environmental Science & Technology 43, 3061–3066. http://dx.doi.org/10.1021/es8020155.

Wei, Y., Zhang, Q., Thompson, J.E., 2013. Atmospheric black carbon can exhibit enhanced light absorption at high relative humidity. Atmospheric Chemistry and Physics Discussions 13, 29413–29445. http://dx.doi.org/10.5194/acpd-13-29413-2013.

Wu, C., Ng, W.M., Huang, J., Wu, D., Yu, J.Z., 2012. Determination of elemental and organic carbon in PM2.5 in the Pearl River Delta Region: inter-instrument (sunset vs. DRI model 2001 thermal/optical carbon analyzer) and inter-protocol comparisons (IMPROVE vs. ACE-Asia protocol). Aerosol Science and Technology 46, 610–621. http://dx.doi.org/10.1080/02786826.2011.649313.

Xiao, R., Takegawa, N., Kondo, Y., Miyazaki, Y., Miyakawa, T., Hu, M., Shao, M., Zeng, L.M., Hofzumahaus, A., Holland, F., Lu, K., Sugimoto, N., Zhao, Y., Zhang, Y.H., 2009. Formation of submicron sulfate and organic aerosols in the outflow from the urban region of the Pearl River Delta in China. Atmospheric Environment 43, 3754–3763.

Xing, J.H., Takahashi, K., Yabushita, A., Kinugawa, T., Nakayama, T., Matsumi, Y., Tonokura, K., Takami, A., Imamura, T., Sato, K., Kawasaki, M., Hikida, T., Shimono, A., 2011. Characterization of aerosol particles in the Tokyo Metropolitan area using two different particle mass spectrometers. Aerosol Science and Technology 45, 315–326. http://dx.doi.org/10.1080/02786826.2010.533720.

Yu, H., Wu, C., Wu, D., Yu, J.Z., 2010. Size distributions of elemental carbon and its contribution to light extinction in urban and rural locations in the Pearl River Delta Region, China. Atmospheric Chemistry And Physics 10, 5107–5119. http://dx.doi.org/10.5194/acp-10-5107-2010.

Zauscher, M.D., Wang, Y., Moore, M.J.K., Gaston, C.J., Prather, K.A., 2013. Air quality impact and physicochemical aging of biomass burning aerosols during the 2007 San Diego Wildfires. Environmental Science & Technology 47, 7633–7643. http://dx.doi.org/10.1021/es4004137.

Zhang, G., Bi, X., Li, L., Chan, L.Y., Li, M., Wang, X., Sheng, G., Fu, J., Zhou, Z., 2013a. Mixing state of individual submicron carbon-containing particles during spring and fall seasons in urban Guangzhou, China: a case study. Atmospheric Chemistry And Physics 13, 4723–4735. http://dx.doi.org/10.5194/acp-13-4723-2013.

Zhang, G., Bi, X., Chan, L.Y., Wang, X., Sheng, G., Fu, J., 2013b. Size-segregated chemical characteristics of aerosol during haze in an urban area of the Pearl River Delta region, China. Urban Climate 4, 74–84. http://dx.doi.org/10.1016/j.uclim.2013.05.002.

Zhang, R.Y., Khalizov, A.F., Pagels, J., Zhang, D., Xue, H.X., McMurry, P.H., 2008. Variability in morphology, hygroscopicity, and optical properties of soot aerosols during atmospheric processing. Proceedings of the National Academy of Sciences of the United States of America 105, 10291–10296. http://dx.doi.org/10.1073/pnas.0804860105.